Journal of Environment and Earth Science
ISSN 2224-3216 (Paper) ISSN 2225-0948 (Online)
Vol.4, No.4, 2014

Geological and Structural Interpretation of Part of the Buem Formation, Ghana, Using Aerogeophysical Data

Kenny M. Graham[1], Kwasi, Preko[2*], David D. Wemegah[2], Daniel Boamah[3]

1. Schlumberger Geosolutions Field Geophysicist, Schlumberger Petrotechnical Service.
2. Department of Physics, Kwame Nkrumah University of Science and Technology, University Post office, Private Mail Bag, Kumasi, Ghana.
3. Geochemistry and Laboratories, Geological Survey Department, Accra, Ghana

*Email of corresponding Author: kwasipreko.sci@knust.edu.gh, kpreko@yahoo.com

Abstract

Airborne magnetic and radiometric datasets were processed to interpret the geology of part of the Buem formation and estimate the depth to basement of magnetic source in the area. The study was aimed at mapping lithology, delineating structural lineaments and their trends as well as estimating the depth to magnetic source bodies of the area. The data processing steps involved advance improved enhancement filters such as reduction to the pole, analytic signal and first vertical derivative, Tilt angle derivative and these helped delineate geological structures and lithology within the Buem formation. The radiometric datasets displaying the geochemical information on potassium, thorium and uranium concentrations within the study area proved valuable in delineating the Buem shales, sandstones, basalts and part of the Voltaian sediments that underlie the Buem formation of the area. Lineament analysis using the rose diagram showed that the area is dominated by north-south (NS) and east-west (EW) trending lineaments. Depths to the magnetic source bodies were estimated using Werner deconvolution method, indicating two depth source models. The depth of the magnetic body produced from the dike model ranged from 101.15 m to 1866.34 m and that of the contact model ranged from 100.36 m to 983.709 m.

Keywords: Buem formation, aeromagnetic, radiometric, hydrothermal, alteration, mineralization.

1. Introduction

The Buem formation of Ghana forms part of the Pan-African mobile belt (Dahomeyide Chain on the southeastern flank of the West African Craton) (Kesse, 1985). They have been regarded as an ophiolite complex indicating a continental collision origin for the Dahomeyide (Kennedy, 1964). The study area and its environs have been surveyed and studied by several geoscientists, particularly for the surface underlie the Buem formation al mapping and geochemical studies. The subsurface geological mapping has less been performed in the study area by integrating geological records and geophysical data. Irrespective of this, only a little attempt has been made so far to understand the detailed relationship between structural features observed on the ground and those extending into the subsurface. Osae et al., (2006) also investigated the petrography, as well as major and trace element of the Buem sandstone and determined their provenance and tectonic setting. Jones, (1990) performed field and geochemical investigation of the Buem volcanic and it associate sedimentary rocks and showed the various lithological unit and how they dip. Affaton et al., (1997) studied extensively on the metamorphosed igneous rocks intercalated within the metasedimentary sequences of the Buem Structural Unit (BSU) and their chemical composition. Norman, (1969) also performed a field and geochronological investigation of the Buem formation and its environs and showed that the Buem and the Togo Formations, which in the past considered being of different ages, can now be classified as a single sedimentary unit. The study area has high rugged topography and dense vegetation coverage which restricts direct geological studies and delineation of the subsurface structure. Thus, the determination of subsurface geology is fundamentally dependent on the use of regional geophysical survey such as airborne geophysical survey. Airborne geophysical survey has been a very useful tool available to Earth scientists in interpreting geology of such difficult terrain (Gunn, 1997). The broad view of the Earth that the airborne geophysics perspective provides has been well recognized since the early days of balloon photography and military reconnaissance (Dobrin and Savit, 1988). Aeromagnetic survey has proved essential in displaying the spatial distribution and relative abundance of magnetic minerals and nonmagnetic minerals in the upper levels of the crust which can help in the visualization of the geology and geological structures of the upper crust of the earth (Gunn, 1997). Airborne radiometric survey on the other hand measures the natural radiation in the earth's surface, which can give the distribution of certain soils and rock type formation and normally shows a good correlation between patterns in the radiometric

data and un-weathered rocks. Based on this, aeromagnetic and airborne radiometric data of the area (part of the Buem formation, Ghana) was processed to delineate the lithology and geological structures of the area. This paper was aimed at processing aeromagnetic and radiometric data to study major surface and subsurface structures, and their relationship with surface structural features in the study area. Interpretation of the processed geophysical data was carried out by the integration of aeromagnetic data, radiometric data, GIS geological information and published literature. A new interpretation (detailed geological map) would be generated showing magnetic units and structures, and the model of subsurface structures present in the area of study. Attempt was also made to estimate the depth to basement of the magnetic body.

The study area under investigation, which covers about 2380 square km, located at latitudes 7º 0' 18.0" N to 7º 40' 33.6" N and longitudes 0º 8' 45.6" E to 0º 30' 3.6" E (Figure 1a). The area encompasses part of the Hohoe, Kadjebi, Kpandu and Krachi district which covers most of Buem Traditional Area and located in the mid-east portion of the Volta Region of Ghana.

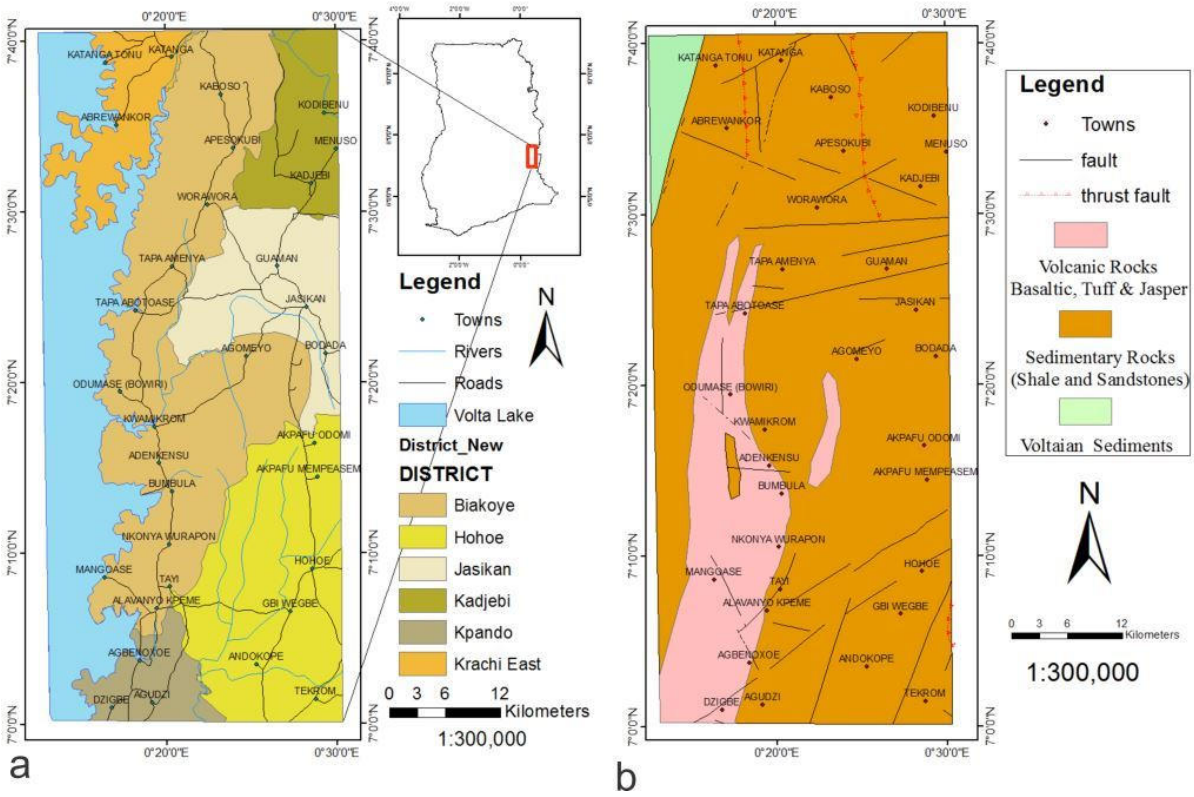

Figure 1. (a) Map of the Study area. (b) Geology map of Study Area.

1.1 Geologic Setting

Most part of Ghana falls within the West African Shield and main rock units underlying the country are the Birimian, the Tarkwaian, the Dahomeyan Systems, the Togo Series and the Buem Formation. The regional geological setting of the study area shown in Figure 1b is a modified geological map after GSD (2009). The study area is mainly dominated by the Buem Formation which defines the eastern limit in Ghana of the Voltaian Basin forms part of the Dahomeyide Chain on the southeastern flank of the West African Craton. The formation consists of a thick sequence of shale, sandstone, and volcanic rocks with subordinate limestone and conglomerate (Dapaah-Siakwan and Gyau-Boakye, 2000). Volcanic formations, of alkaline to calc-alkaline affinity, are interbedded in the formation (Delor, et al., 2009). In general, the rocks of the Buem Formation are not metamorphosed, and deformation is expressed as the result of thrust tectonics with development of imbricated thrust systems and duplexes. The deformation in the Buem Formation includes large-scale thrusting towards the west (Wright et al, 1985). Folds are not well developed but are expressed as chevron folds in the finest grained material. Close to their contact, the area is folded and metamorphosed with the Togo series and the Voltaian formation. It is acknowledged that infill material of the Buem was probably derived from the Voltaian

Basin and from the Togo Group (Delor, et al., 2009). The volcanic group of rock occurs along the western margin of the study area (Figure 1b). The volcanic group includes many closely intermingled volcanic rock types: various facies of basalts, microgabbros, andesites and jasper (Geotech Airborne Limited, 2009). The jasper in the area (around Kwamekrom) are interbedded with some iron oxide content (Jones, 1990) The volcanic rocks are better exposed on the Abutor Hill Range southwest of Kwamekrom and in stream valleys northwest and southwest of Odumasi. Two volcanic rock types occur in the area, namely, agglomerate and amygdaloidal basalt, which exhibit pillow lava structure (Blay, 2003). The sandstone group include medium-to coarse-grain feldspathic sandstones, quartzitic sandstones, gritty quartzites, quartz-schist and poorly exposed conglomerate and are frequently cut by quartz veins (Jones, 1990). Minor thin band of variably-coloured shales and siltstones occur interbedded with the sandstone. These sandstones are also deformed and brecciated. They contain clayey and other rock fragments (Osae et al., 2006). Generally, the sandstone rocks outcrop in the graphically higher ground (Blay, 2003). Junner (1940) believed that the sandstones of the Nkonya hill land are strongly folded and showed greater dips than the volcanics. This argillaceous (shale) group are of massive shaly rock with interbedded siltstones, thin-bedded sandstones and impure limestone members. Minor shale is found to be interbedded with the Buem sandstones in some places. The Buem argillaceous rocks are restricted to lower topographic level and in stream valleys where they are better exposed (Blay, 2003). The only sedimentary structures seen in the shales were dessication cracks and ripples west of Kwamikron (Jones, 1990). The rocks are generally not metamorphosed except towards their boundary with the Togo and the Voltaian (Blay, 2003).

2. Materials and Methods

2.1 Datasets

Airborne geophysical survey data acquired in 1997- 1998 by the Geological Survey of Finland (GKT) in collaboration with the Geological Survey of Ghana and the Ghana Minerals Commission was processed for this studies. The area was surveyed using a fixed wing aeroplane (Cessna Titan 404 (C-FYAU)). The magnetic system used was the Scintrex Cesium SC-2 magnetometer coupled with helium sensor. The output from the magnetometer was sampled at 0.2 s to a resolution of 0.01 nT with noise envelope of 0.1 nT. The sensor was kept at a constant height of 70 m above the ground and measurement were taken every 8 m. The Exploranium spectrometer, model GR-820 with 256 spectral channels and Exploranium detector GPX-1024, 1024 cubic inches of NaI (Tl) (Sodium iodide crystals treated with thallium) coupled in the aero-plane were used for the radiometric data collection. Sampling was done every 80 m. The Global Positioning System (GPS) was used for navigation. The nominal line separation was 400 m with tie lines at approximately 5 km intervals and terrain clearance of 70 m. The survey direction was chosen (East-West) to intersect the main geological strike direction of the area (South- North) perpendicularly. Beside the aeromagnetic and airborne radiometric data, digital elevation and available GIS data, both published and unpublished was used for integration and interpretation.

2.2 Data Processing

Processing of airborne dataset involved the application of advance improved enhancement technique, the application of a gridding routine, and removal of the earth's background magnetic field. Corrections like background correction (aircraft, radon and cosmic), stripping, microlevelling, removing diurnal variation of the earth's magnetic field, aircraft heading, instrument variation, lag error between aircraft and the sensor and inconsistencies between flight lines and tie lines were done by the Geological Survey of Finland (GKT) (the contractors) . The datasets were equally spaced in a 100-meter square grid cells, using a minimum curvature interpolation algorithm (Briggs 1974). This procedure allowed for immediate application of the proposed filtering and enhancement techniques. The grids of the residual magnetic anomaly and that of K, Th and U were microlevelled using a routine developed by Blum (1999). The microlevelling corrected the small inconsistencies and spatially homogenizes in the data and made it possible to generate a better image for analysis. The geophysical data set for the study area was co-registered to Universal Transverse Mercator (UTM) Coordinate System, zone 31 of North hemisphere. The main software used for the processing and enhancement of the airborne geophysical data were the Geosoft® (Oasis Montaj) and the Discover 12. The ArcGIS was used to create the GIS environment for the integration of the interpreted results.

Processing steps with the magnetic dataset involved advanced improved enhancement filters such as reduction to the pole, analytic signal and first vertical derivative, Tilt angle derivative. These enhanced the geological features, thus helping to delineate the geological structures and lithology within the Buem formation. Magnetic

intensity generated from the profile to grid data was then displayed as an image in natural colour pallets (magenta high intensity, blue low intensity) using histogram equalization to maximize the colour ranges. Since there was a substantial change in magnetic intensities from the inclination and declination at low latitudes, it was vital to define the magnetic anomalies at the place where they sit over the source. Mathematical transformation or filtering techniques, such as reduction to the pole, RTP and analytic signal, was applied to place the magnetic anomaly as if it sits over the magnetic source. Most linear anomalies of the study area were not revealed by gridded residual intensity magnetic imagery. Processing using vertical derivative and automatic gain control filters removed the influence of the large amplitude, long wavelength anomalies and reveals the linear anomalies. Upward continuation filtering aided in the determining the depth range of deeper magnetic sources. Edge-detection filters are normally applied for delineating linear features without necessary diminishing the long-wavelength anomalies (Oruc and Selim, 2011). For this reason, the Tilt derivative filter, TDR (a very good edge-detection filter) was applied to bring out short wavelength and reveals the presence of magnetic lineaments. The grids of each gamma-ray spectrometric channel were then microlevelled using a routine developed by Blum (1999). The microlevelling algorithm filtered out most of apparent residual error remaining after the application of the standard survey grid techniques and also corrected the small discrepancies and spatially homogenizes the data (Elton et al., 2003). A histogram equalization to give the best colour variation was used to enhance the contrast of the individual histograms of K, Th and U before combining to generate the ternary image. The Geosoft® oasis montaj software was used to generate the ternary RGB colour model for which potassium, thorium and uranium were assigned to the red, green and blue respectively. The ternary image generated showed the best visual description of the radiometric intensity which correlated well with the geological features in the area.

Attempt was also made to estimate the depth to basement of the magnetic body. The Geosoft oasis montaj *Depth to Basement extension* which determines the position and intensity (susceptibility) of magnetic source bodies for a magnetic profile was used. The *Werner Deconvolution* function uses the horizontal and vertical derivatives in the calculation of the depth to basement of the magnetic anomaly. *Werner Deconvolution* function assumes the source bodies were either dikes or contacts with infinite depth extent and uses a least-squares approach to solve for the source body parameters in a series of moving windows along the profile (Ku and Sharp, 1983). The anomaly profiles selected (thee profiles) were perpendicular to the geological structure generating the field.

2.3 Interpretation Methods

Interpretation of the dataset was carried out manually, based on the variations in texture and amplitude of the datasets with particular attention paid to delineating the lithology and geological structures of the area. The interpreted aeromagnetic and airborne radiometric data were integrated with others GIS data for mapping lithology and geological structures in the study area. Domain boundaries and structural features, such as folds, faults and thrusts, and lithological contacts were also digitized. The improved enhanced aeromagnetic maps were used to distinguish the magnetic responses in the bedrock geology due to the difference in magnetic susceptibilities, structures and deformation styles of the magnetic units in the area. The first step in the analysis and interpretation of radiometric data consists of a visual interpretation of the single channel information, followed by analysis of the ternary map.

3. Results and Discussion

3.1 Interpretation of Aeromagnetic Dataset

RMI map displays different regional magnetic zones (BV, BS, BSH, C and VS in Figure 2a), with most of them trending in the north-south direction and some been polygon features (BS, VS). Residual magnetic intensity level in the study area ranges from -922.27 to -1515.95 nT with the mean value of -1256.33 nT. The negative anomalies observed in the area was attributed to the present of low magnetic rocks (e.g. shale, sandstone, limestone) in the area, that were noted for its low magnetic signatures. Thus removing the regional magnetic anomaly from the total magnetic intensity produced these negative values. Magnetic zone division was based on the intensity, shape, and pattern in magnetic signatures. At the west lower corner zone, there exists a high magnetic signature zone (BV Figure 2a) which is cut by low magnetic signature (VS in Figure 2a). This intruding body VS (low magnetic signature) that cuts the BV body was suspected to be sediments from the Voltaian basin which is known to have low magnetic signature. The high magnetic intensity body, BV, observed at the lower left corner of Figure 2a was interpreted as the Buem Volcanic rocks which were known for its high magnetite content (Jones, 1990). The most prominent relatively low magnetic intensity with a polygon feature was observed at the central zone (BS in Figure 2a) of the area. This feature, BS, observed at the lower side of the

map was interpreted as the Buem sandstone (Osae et al., 2006). The relatively high magnetic signature observed in the sandstone (BS in Figure 2a) was described by Osae et al., (2006). He indicated that the sandstone has some iron oxide element in them and this may explain its relatively high magnetic signature. Relatively low anomaly (BSH in Figure 2a) with intensities ranging from -1254 to 1246 nT was also observed just close to the circular feature (BS in Figure 2a). This feature, BSH, which was also observed around BS and VS, was delineated as the well-known Buem shale described by Jones (1990). Jones (1990) described the shale in the area to be noted of having low magnetite content hence producing low magnetic signature.

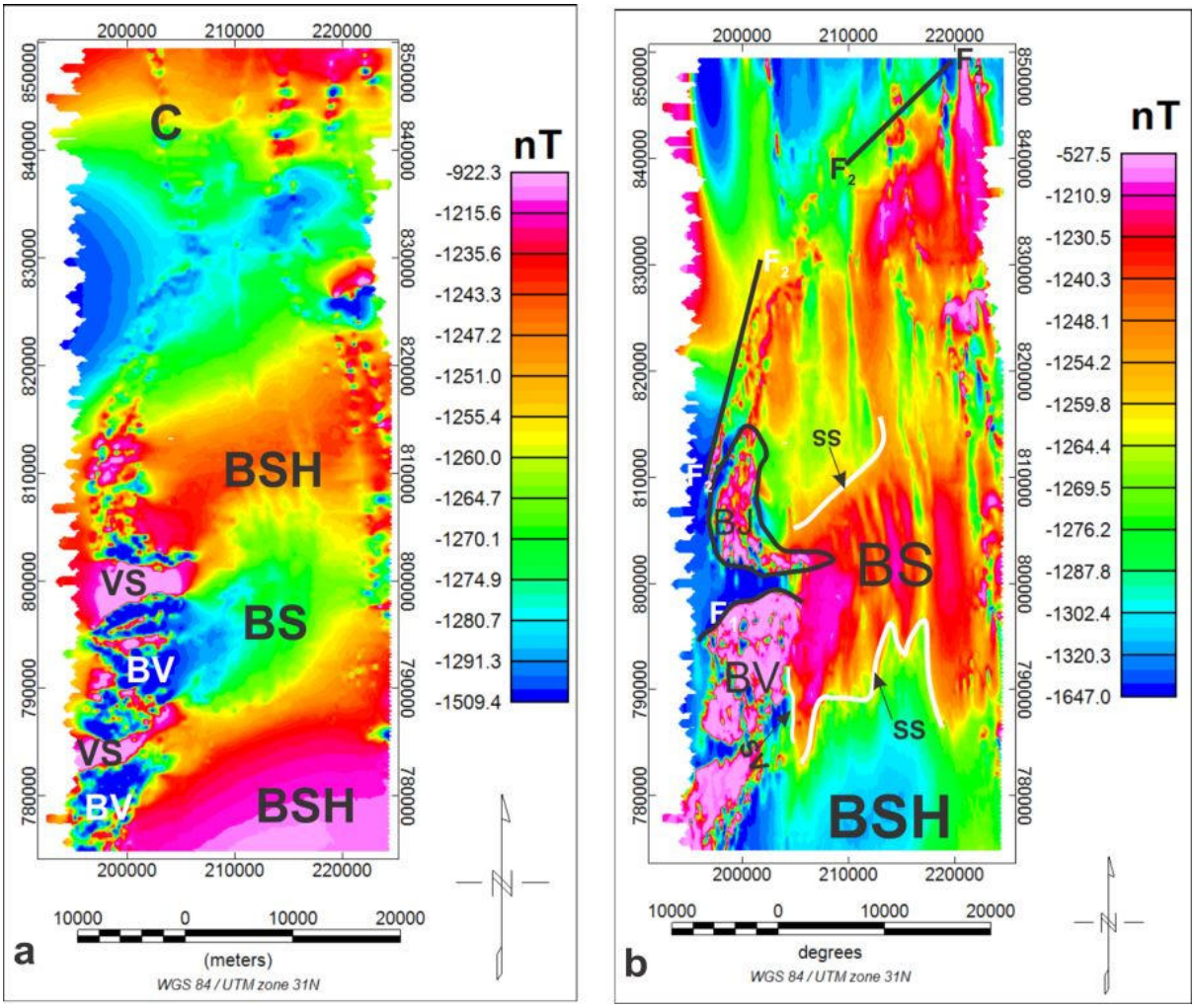

Figure 2. (a) Residual Magnetic Intensity, RMI grid map. (b) Reduction to the pole (RTP) image (using an inclination of -11.1 and declination of -4.9^{o}.

Reduction to the pole, RTP filter was applied to the RMI grid to observe the magnetic anomaly directly over the magnetic source bodies that cause the anomaly and also to remove the influence of magnetic latitude on the residual anomalies. Both RMI (Figure 2a) and RTP image (Figure 2b) displayed similar magnetic features, but in the RTP grid, the high anomalies of the RMI grid were seen as low while the low anomaly are seen as high. This observation was attributed to the area (low magnetic latitude) where the data was acquired. At low magnetic latitude, high magnetic signatures are normally observed as low signatures and vice versa (Gunn et al., 1997). The RTP map show more significant features such as structures and lithology than the RMI grid. At the centre zone (BS in Figure 2b) some features observed in the RMI were now seen as linear features trending in the south-north direction. Moreover, other features (e.g. the low magnetic signature (VS in Figure 2b) and high magnetic signature (BV in Figure 2b)) which were not clearly seen in the RMI image (Figure 2a) were seen in the RTP. Interestingly, some high (pink) features in the RMI image remained high (pink) in the RTP image. This may be to the fact that the magnetization of the causative body may not be as a result of remnant magnetization.

Example was the magnetic signature BJ found at the western part of the area. This feature was interpreted as the jasper in accordance to what Jones (1990) reported. He described the jasper in the area (around Kwamekrom) to be interbedded with some iron oxide content and this iron oxide content may be responsible for the high magnetic signature in that region (BJ). Folding, F1 (in Figure 2b) of the Buem volcanic rock (BV) (located at the south western corner which trends south-northeast) caused by the collision between the Buem formation and the Voltaian formation (Kennedy, 1964) was well defined in the RTP image (Figure 2b). Some magnetic contrasts observed in Figure 2b were interpreted as the lithological contacts. Prominent was the Buem sandstone and the Buem shale contact (white lines, SS in Figure 2b).

The RTP grid was draped over the digital elevation map (DEM) of the area and viewed in 3D (Figure 3a) to help visualize the relation between the magnetic intensity and the elevation of the area. Interestingly, the relatively high magnetic signature (BS) located at the south-central part of the area was seen to have a close relation with the topography of the area. This confirms the description Jones (1990) gave concerning the sandstone in the area as being found in areas of high elevation. Another obvious location where this observation can be clearly seen was the Alavanyo mountain range (Blay, 2003).

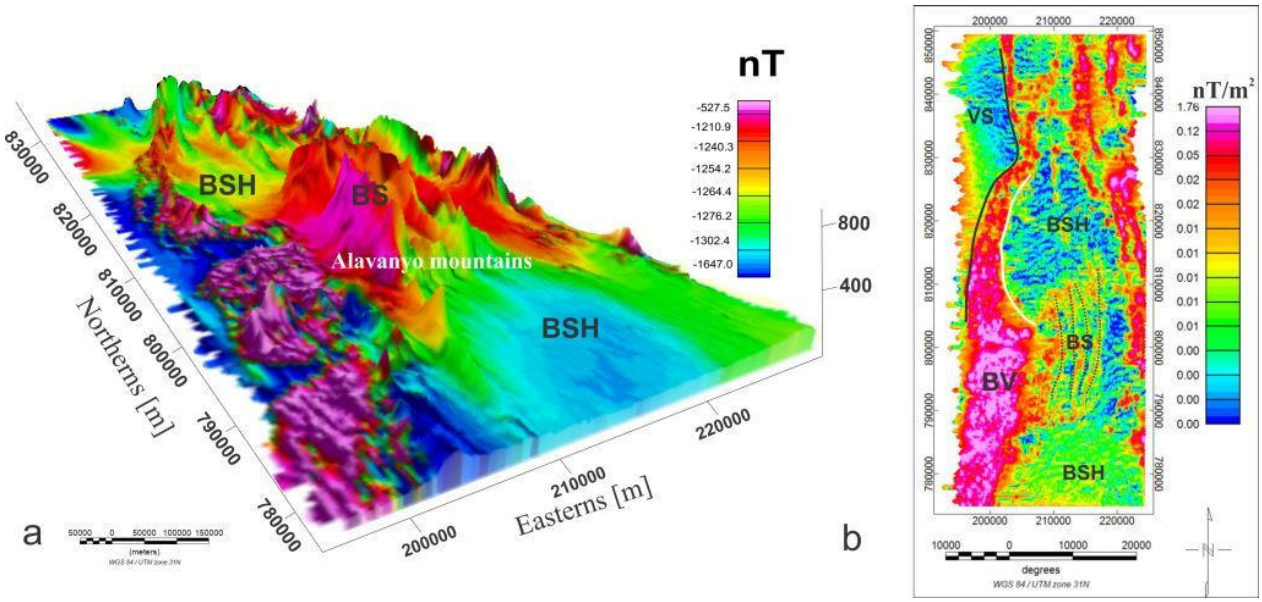

Figure 3. (a) RTP drape over DEM viewed in 3D (Red - high magnetic signature and blue- low magnetic signature). (b) Analytic signal image.

The analytical signal, AS, filter was applied to the RMI grid to observe the source positions of the magnetic anomaly regardless of direction and remnant magnetization in the sources since analytical signal is independent of the direction of the magnetization of the magnetic source. Figure 3b (analytical signal map) shows that, most prominent features, the high analytic signal amplitude runs in an approximately south–north (SN) direction along the western border of the area. Three major magnetic zones i.e. high magnetic anomalous zone define by (BV), intermediate magnetic anomalous zone (BS) and low magnetic anomalous zone (BSH and VS) were delineated (Figure 3b). The high magnetic signatures (BV) of the analytical map were the volcanic rocks (Bell and Crook, 2003) which were found around the south-western part of the area and trend in the south–north direction (Figure 3b). Lithological contacts portrayed by a sharp magnetic contrast were delineated; prominent among them were the volcanic-shale contact (white line in Figure 3b) and the Buem-Voltaian contact (black line in Figure 3b). Osae et al., (2003b) described the outcrop of the Buem sandstone as having a lens-shape body (thick in the middle and thin at the edge) and overlap in lines to form a range of hills. This description of the sandstone was shown in figure 3b as doted black lines around BS.

The TDR filter was applied to the RMI and the RTP grid to determine structures (fault and folds), the contacts and edges or boundaries of magnetic sources, by enhancing both weak and strong magnetic anomalies and to see the near surface source magnetic features that were associated with geological structures of the area. Tilt angle derivative (TDR) of RMI helped locate the edges of formations, especially at shallow depths by using the theory that the zero contours are the edges of the formation (Salem et al., 2007). It was observed that the zero contours

estimate the location of abrupt changes in magnetic susceptibility values. The zero contour lines in this grid (Figure 4b) were represented by a yellow colour.

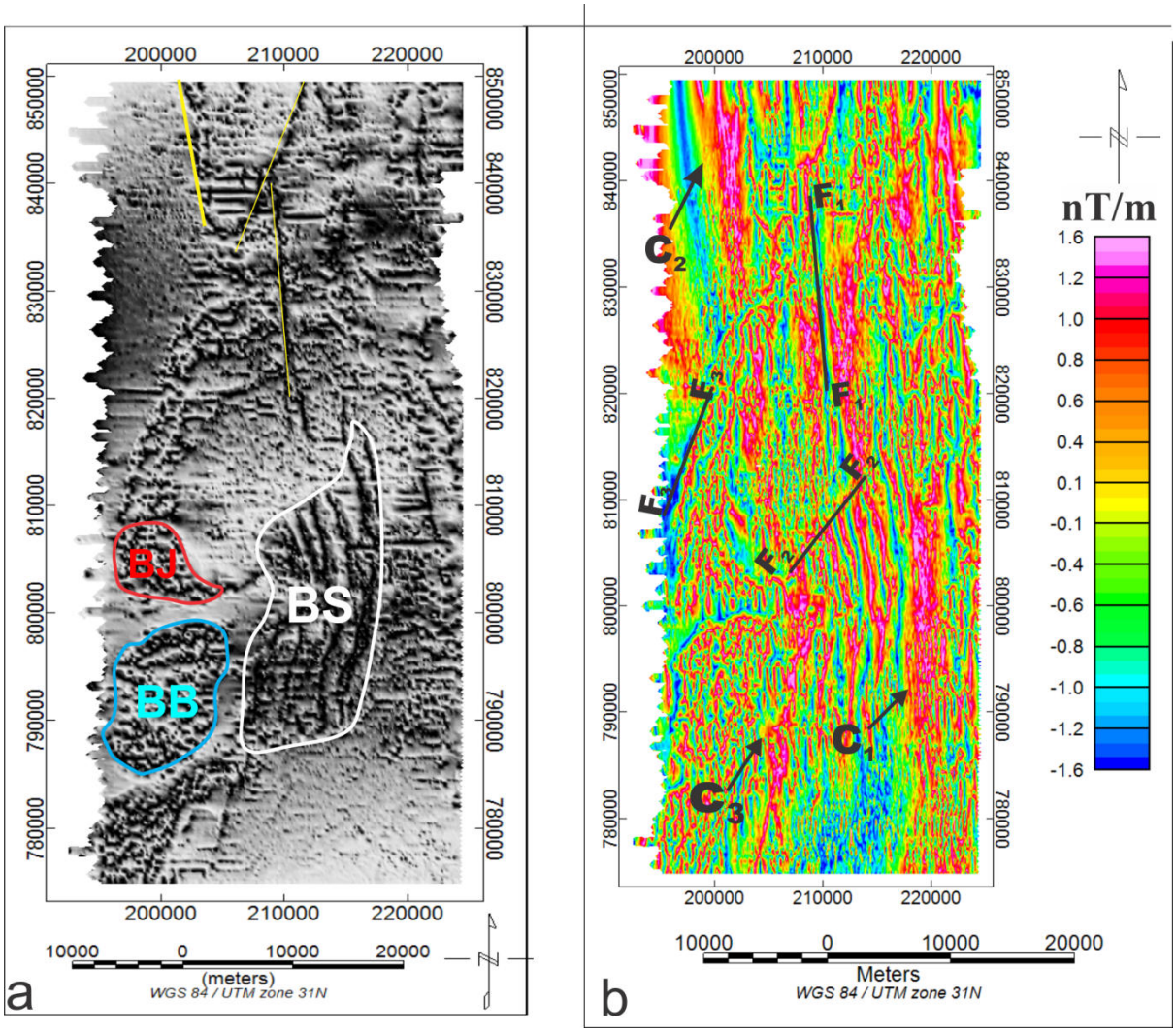

Figure 4. (a) TDR calculated from RTP image. (b) TDR calculated from RMI.

Figure 4a displays most structural feature of the area such as the faults, inferred faults, contacts, and to some extent the shape of some lithology. Some lithological unit (e.g. BJ, BB and BS in Figure 4a) in the area are accentuated. Prominent of these features are the ones marked with blue polygon, BB (in Figure 4a) at the south-western part of the area and this was interpreted as the basalt with some associated volcanic rocks as described by Jones (1990). The jasper which Jones (1990) described to be around Kwamekrom was clearly delineated (marked with a red polygon, BJ, in Figure 4a). The delineated jasper had an area cover of about 9388 m^2 (square meter). Junner (1940) reported that the sandstones in the area to be strongly folded and showed greater deformation (faulted) than the Buem Volcanics. This observation is accentuated in the TDR image (BS in Figure 4a). This feature, BS, believed to be the Buem sandstones was seen to be highly faulted and deformed. This deformation and folding was as a result of the thermo-tectonic event that occurred about 600 m.a ago (Jones 1990). The linear anomalies believed to be thrust faults were also seen at the northern part (marked with yellow line in Figure 4a) of the area. According to Jones (1990) these thrust faults relates to the eastern Pan- African orogenic event which occurred several years in the northern part of the study area. TDR image (Figures 4a and 4b) also show different lineaments and contacts in the area. Prominent lithological contacts observed are; the shale-sandstone (C1), the Buem-Voltaian (C2) and the Volcanic-Shale (C3) in Figure 4b. Some structural lineaments (faults) e.g. F1, F2 and F3 were delineated by observing the abrupt change between the positive and negative magnetic anomalies (Figure 4b).

Figure 8 shows the interpreted geological structures in the area delineated from the magnetic dataset and superimposed on the TDR image. These structures were integrated with the information from the RMI grid

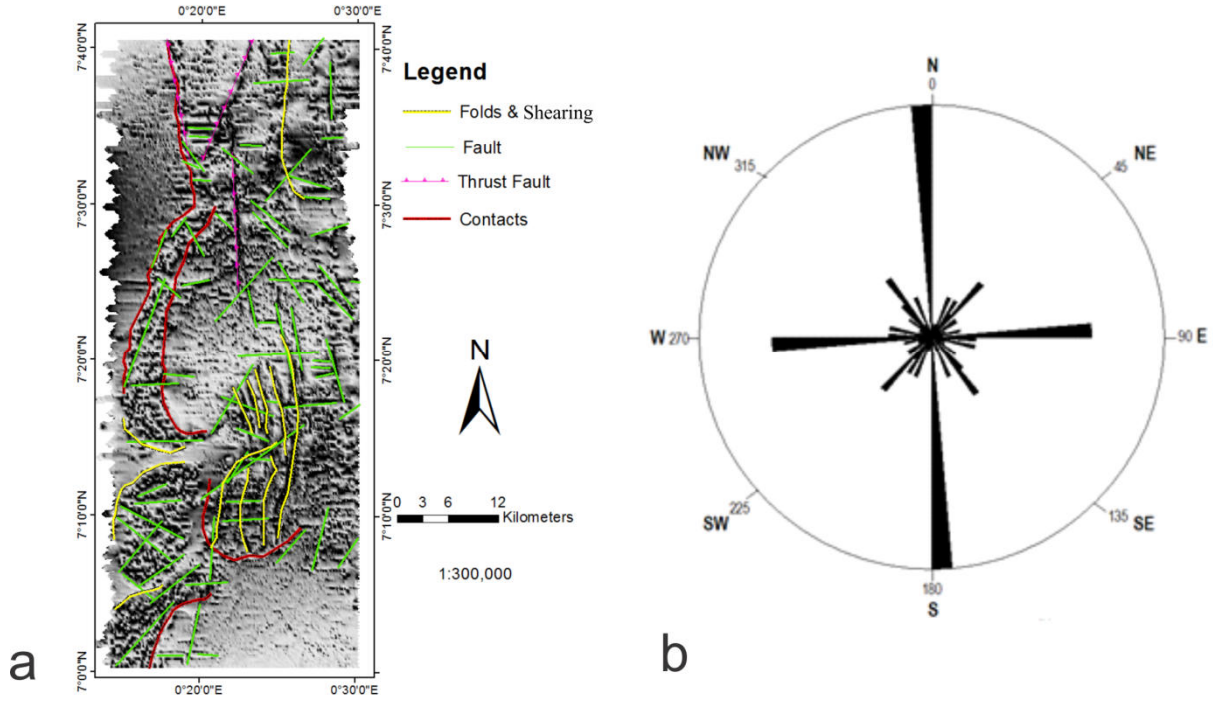

(Figure 2a), RTP grid Figure 2b, analytical signal grid (Figure 3b) and TDR grid (Figure 4a). The map gave a rough idea about the geological structural control and lithology deformation of the area. It shows the high structural deformation (folding and shearing) in the Buem sandstones.

Figure 5. (a) Interpreted fault, folds and contacts superimposed on the TDR image. (b) Rose diagram showing the lineaments orientation of the study area.

The orientation and the length of the lineament extracted from aeromagnetic images were displayed in a rose diagram to analyse the spatial distribution of lineaments and in order to contribute to the understanding of the structures of the study area. The rose diagram (azimuth-frequency), Figure 5b, shows trends in north south (N-S), east-west (EW), northeast southwest (NE-SW) and northwest southeast (NW-SE) direction. Out of the 80 extracted lineaments, 21 % (representing the largest) trends in the NS direction with 11% striking in the EW direction. 6% also strikes in the northeast southwest (NE-SW) and another 6 % trending in the northwest southeast (NW-SE) direction. The area was dominated by a series of SN and EW trending structures and are interpreted as higher degree of shearing and faulting may have been formed during thermo-tectonic activity in the Buem volcanic formation (Kennedy, 1964).

3.2 Interpretation of Radiometric Data

Airborne radiometric survey measures the spatial distribution of three radioactive elements (potassium-K, thorium-Th and uranium-U) in the top 30-45 cm of the earth's crust (Gregory and Horwood, 1961). The abundances of K, eTh and eU are measured by detecting the gamma-rays produced during the natural radioactive decay of these elements. Changes in the concentration of the three radioelements eU, eTh, and K accompany most major changes in lithology; hence the method has been used as a geological mapping tool in many areas (Wilford et al., 1997). On regional scale airborne gamma-ray spectrometry data have often been used to identify several features, such as: limits of geological provinces, sedimentary basin and overprinted structural trends (Direen et al., 2001). It has also proven to be a useful method for the study of geomorphology and soils. The area was divided into radiometric domains (regions) based upon the concentration, shape and abrupt change of radiometric concentration in the radiometric image. Boundaries of the individual lithological domains are seen as abrupt changes in the radiometric concentration.

From Figure 6a, low potassium concentration was observed at the left side of the grid (VL), and similar observation was seen at the upper left corner of the area. This observation coincides with the Volta Lake (Figure 1a) which was observed in the study area. Low concentration was recorded because water body adsorb the potassium radiation form the underlying rocks preventing the radiations from been detected by the spectrometer. Since radiometric survey uses the assumption of residual of soil and the top 30 cm soil was able to adsorb most of the radiated radioactive element from the underlying rocks or the lithology. High concentration of K was also observed at the south-west corner (B in Figure 6a) of the area. B was suspected to be basalt described by Jones (1990); Osae et al., (2006) as being alkaline and having high concentration of K. High concentration of potassium concentration was found at the central (BSH in Figure 6a) part of the area. This coincides with the shale region mapped from the analytical signal map (Figure 3b) of the magnetic data. This shows that the shale in the area has high concentration of K and can be attributed to the description given by Osae et al., (2006) concerning Buem shale. Osae et al., (2006) described shale in the area as emitting more gamma rays than other sedimentary rock in the area.

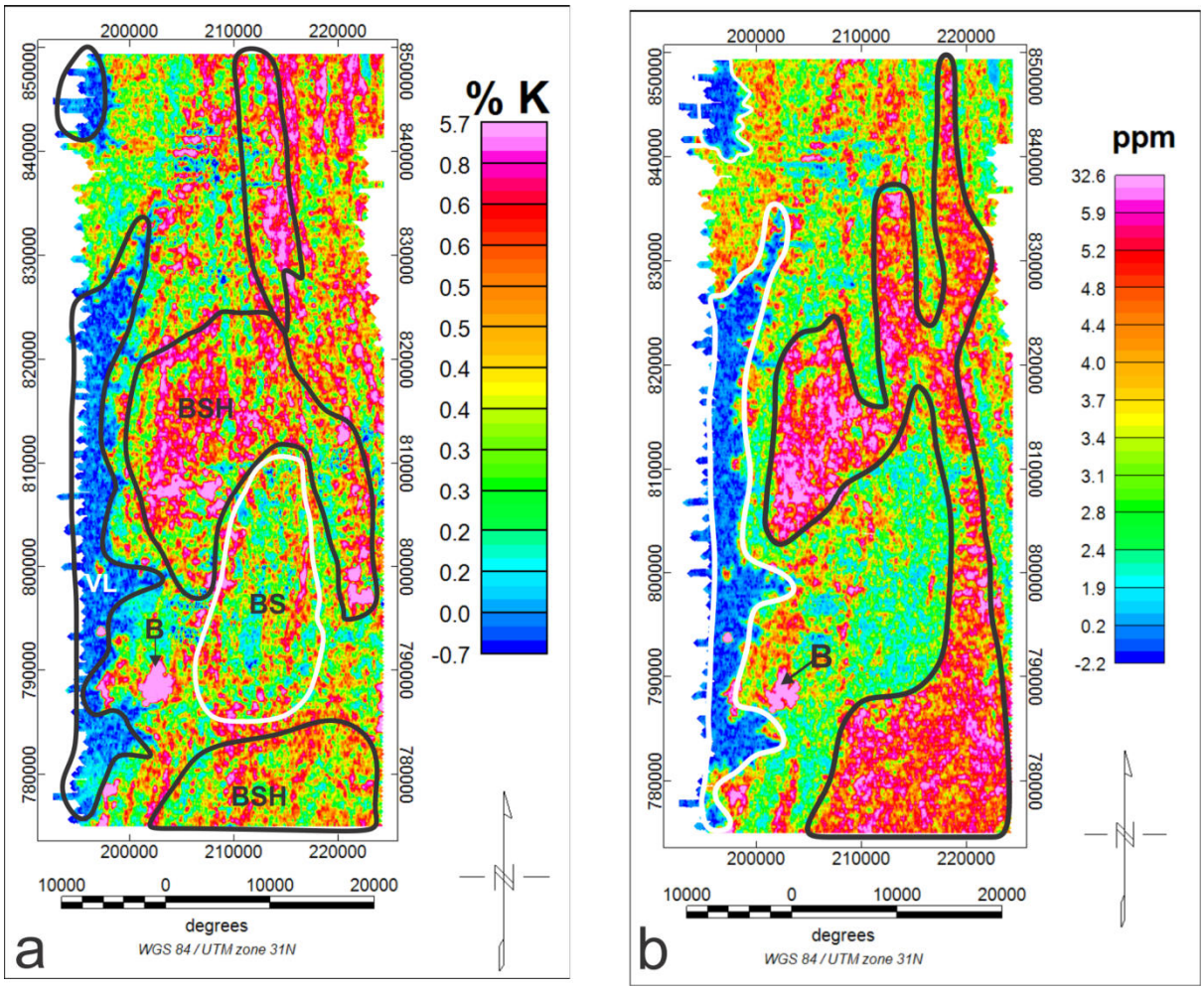

Figure 6. (a) Gamma spectrometric image for Potassium (K) concentration. (b) Gamma spectrometric image for thorium (eTh) concentration.

Anomalies in the thorium data in Figure 6b helped map the lithology and lithological boundaries of the area. The thorium, eTh map shows three distinct regions of thorium concentration in the area. The high concentration in eTh marked by black polygon (Figure 6b) correspond to the shale and other weathered sediment in the area. These weathered sediments are believed to have originated from the rock (sandstone) in the high elevated lands in the region (Jones, 1990). The relatively high concentration of eTh was associated with the sandstone in the area (Figure 2) and this coincides with the high elevated lands in the area. Prominent of this relatively high eTh

anomaly was observed around the Alavanyo high lands. Moreover, the low concentration of eTh marked by white polygon observed at the western part of the area coincides with the Volta Lake in the area. This indicates the fact that the water body may block the emission of radiogenic element (thorium) of the underlying lithology.

The uranium image shows good definition in mapping the Volta Lake (marked by black polygon in Figure 7a) and certain geological formations such as B. The feature B, registered high Uranium concentration. Interestingly, the circular body (B) which was observed in the eTh and Potassium map was also observed in the eU map. The feature coincides with the Basalt which Jones (1990) described to be located around that south western part of the area. Unlike the K and the eTh maps, eU map could not clearly delineate the distinct boundary between most of the lithology of the area. The obvious boundary between the sandstone and the shale which are clearly seen in the eTh map (Figure 6b) and Potassium map (Figure 6a) was not observed the Uranium map. This may be due to the fact that the image (Figure 7a) shows short wavelength anomalies corresponding to noise caused by the variations in atmospheric radon concentrations during the course of the survey resulting in significant streaking in the image. This was a typical feature found in uranium images (Minty, 1997), in spite of the processing steps the dataset was subjected to.

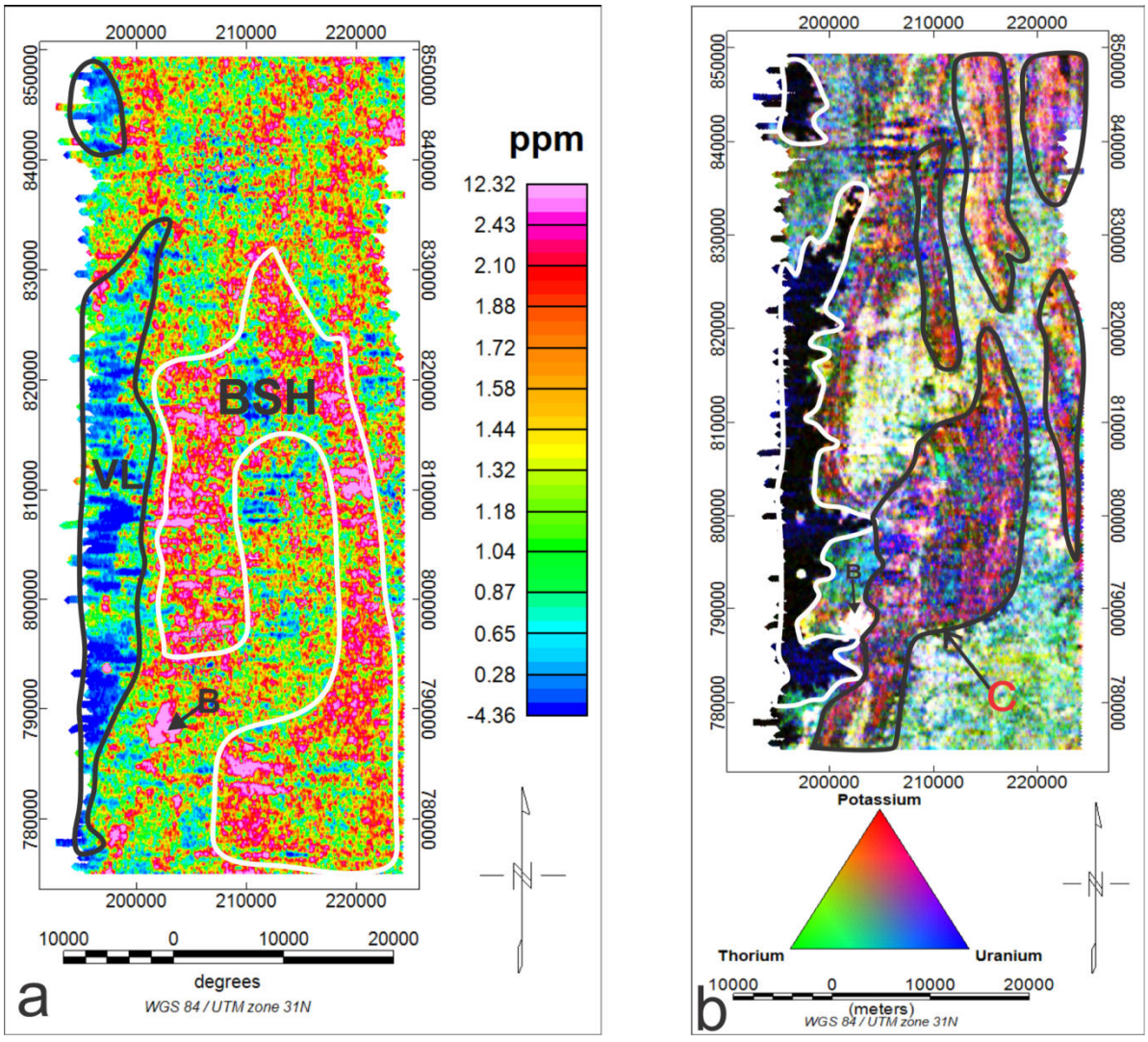

Figure 7. (a) Gamma spectrometric image for Uranium (eU) concentration (b) Ternary map of Study area (RGB=KThU)

The radiometric data are displayed as a ternary map with combined intensities of potassium (K), thorium (eTh), uranium (eU) concentration given in red, green, and blue colour respectively. The radiometric responses in the

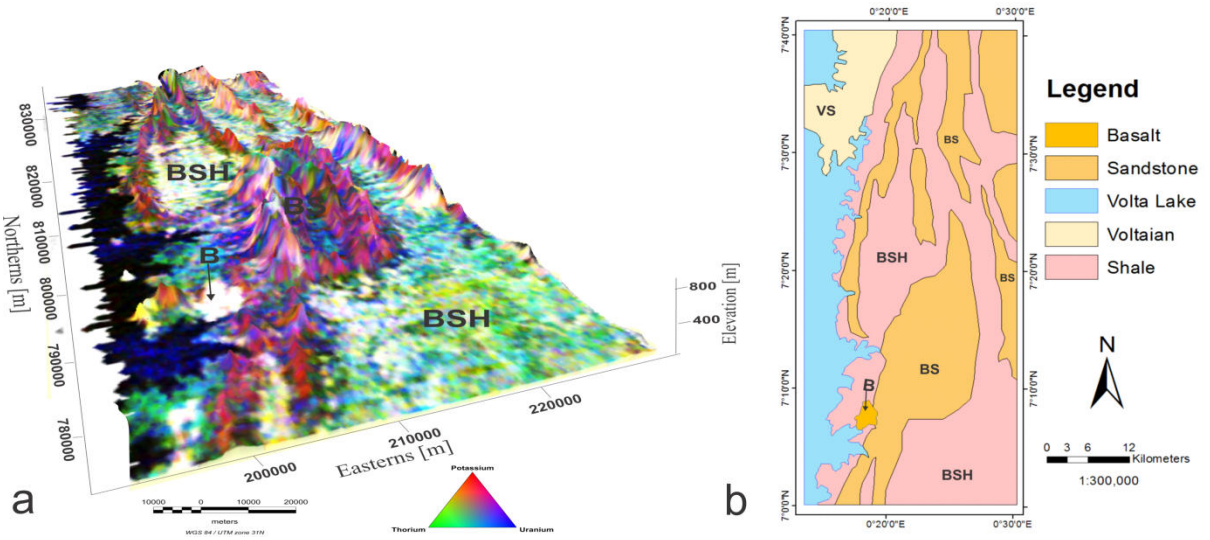

ternary map, to some extent, correspond with the surface geological map of the study area (Figure 1b). From the ternary map, the Volta Lake can easily be delineated as having low concentration of the three radiogenic elements (depicted by a black colour in Figure 7b). The contact between the shale and sandstone (C in Figure 7b) in the area was also observed. The high concentration of K, Th and U, marked with the black polygon coincide with the shale and weathered sediment in the area which Osae et al. (2006) and Jones (1990) described to be in the area. The high K with low U and Th concentration which was depicted by a magenta colour coincides with sandstone in the area and interestingly it also coincides with the high elevated land in the area. Osae et al. (2006) reported that the sandstones in the area are normally found at the highlands or the elevated regions in the area.

Figure 8. (a) Ternary map draped over DEM and viewed in 3D. (b) Interpreted lithological map from the radiometric dataset.

The ternary image was draped with the DEM of the area (Figure 8a) to observe the behaviour the three radiogenic elements, K, U and Th with the elevation. It was observed that the high elevated regions in the area coincided with the high K concentration as well as low U and Th concentration (magenta colour in Figure 8a) and this was interpreted as sandstone. Moreover, lowlands were seen to coincide with high concentration of all the three radiogenic elements, K, U and Th. Information from the Uranium image (Figure 7a), Potassium image (Figure 6a), Thorium image (Figure 6b) and the Ternary image (Figure 7b) alongside published articles and geological map of the area was combined to generate a lithological map of the study area (Figure 8b). Information from aeromagnetic dataset, airborne radiometric dataset and published literature of the area were put together to produce a regional geological map of the study area (Figure 9) which consists mainly of the Buem formation and the Voltaian sediment. The integrated geological map (Figure 9) shows the various lithological units and the geological structures in the area.

It can be observed from this map (Figure 9) that the Buem sandstones (BS) are associated with different regimes of tectonic activities producing faults and folds. This can be attributed to the thermo-tectonic event that occurred within the Buem formation about 600 m.a. (Kennedy, 1964; Jones, 1990; Osae et al., 2006). Most of the delineated structures found within the sandstone, (BS) (at the central and eastern part of the area), volcanic rocks and the basalt (western part of the area) strikes mostly in the N-S and E-W direction.

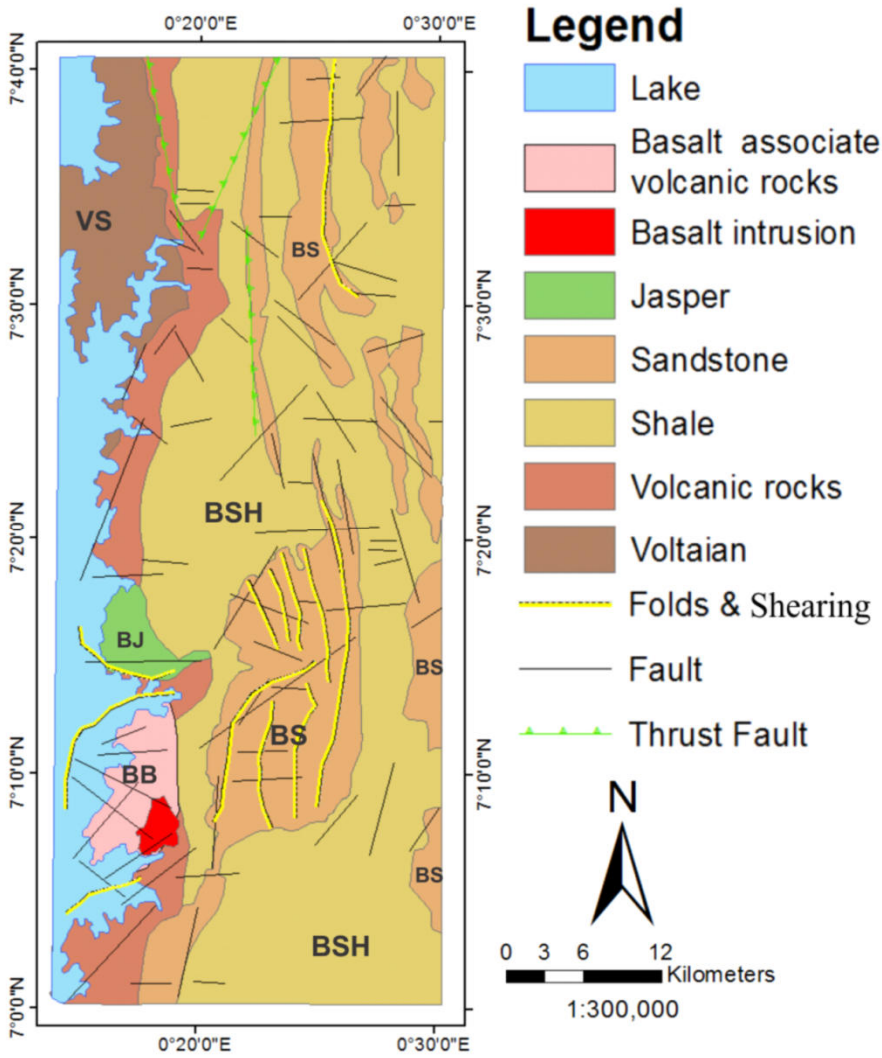

Figure 9. Proposed Geological Map of the Study Area.

3.3 Quantitative Interpretation

Three profiles which are perpendicular to the strike direction (N-S) of the formation were chosen across the residual aeromagnetic intensity map of the area to estimate the depth to magnetic bodies and possibly the intensity (susceptibility). Two depth source models (Dike and contact models) were assumed and their depths to basement were estimated. The profile A-A1 (line 357) was a 30-km section of a flight line which cuts the shale, sandstone and the basalt in the area and runs east to west. 106 solutions were generated with the dike model and the model for the contact generated 72 and 34 solutions respectively for profile A-A1. The depth to basement of A-A1 ranged from 103.11 m to 857.99 m and the magnetic anomaly values varied from -1140.27 nT to -1327.13 nT. The depth to basement of the contact model was shallow (103.11 to 717 m) as compared to the dike model (114.41 to 857.99 m).

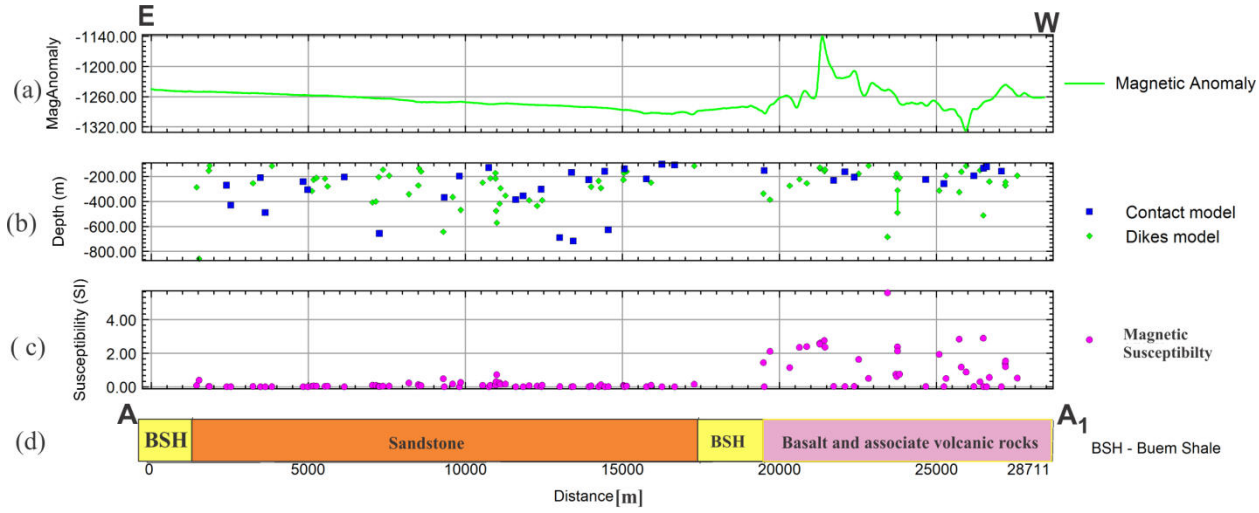

Figure 10. Werner deconvolution solutions from a magnetic profile A-A1 over the study area: (a) residual magnetic intensity profile [nT], (b) depth [m], (c) susceptibility contrast [SI]. (d) A simplified geological section of the interpreted geological map

Table 1. Depth to basement estimation of magnetic body

	Dike		Contact		Magnetic Anomaly (nT)	
	Minimum	Maximum	Minimum	Maximum	Minimum	Maximum
Line 357 Profile (A-A1)	114.41	875.99	103.11	717.33	-1140.27	-1327.13
Line 375 Profile (B-B1)	101.15	1866.34	100.36	983.71	-1214.33	-1397.33
Line 457 Profile (C-C1)	131.00	1605.24	113.82	846.28	-1270.13	-1302.81

From Table 1, it was seen that the depth to basement of the contact model for the three selected profiles was shallow (ranging from 100.36 m to 983.709 m) as compared to the dike model (ranging from 101.15 m to 1866.34 m). This was because dike model anomaly occurs at a greater depth than the contact model (Mushayandebvu et al., 2001). Since the area is mostly of sedimentary rocks the dyke model is the best model for the area.

4. Conclusion

In order to map the lithology and geological structures, map of the study area, airborne radiometric and magnetic datasets collected over the area were processed and enhanced. The magnetic image enhancing filters applied to the residual magnetic intensity (RMI) using reduction to the pole (RTP), analytic signal, first vertical derivative (1VD), Tilt derivative (TDR) and upward continuation (UC). These filters helped define the lithological boundaries, intersection of geological structures, faults, folds and contacts. The Tilt derivative (TDR) proved very useful for the delineation of the contacts and most of geological structures in the area. The radiometric data provided geochemical information of uranium (U), thorium (Th) and potassium (K) and proved valuable in delineating bedrock lithology of the area such as the Buem shale, sandstone, and part of the Voltaian sediments. The radiometric dataset was also valuable in the delineation of the Volta Lake and the lithological contacts of the various rock formations. The interpretation of the high-resolution airborne magnetic dataset has provided a synopsis of the regional geology (lithology) as well as further insight into structural controls of the area. It also shows a detailed assessment of various lithology and north-south striking of the geology in the area. The depth to basement of the formations within the study area was determined using the contact model and the dike models. The contact model produced shallow depth range of 100.36 m to 983.709 m while the dike model on the other hand produced depth range of 101.15 m to 1866.34 m for the basement rock. This was because dike model

anomaly occurs at a greater depth than the contact model (Mushayandebvu et al., 2001). The dyke model seems to best fit the study area.

Acknowledgements

We are most grateful to the Geological Survey Department, Accra, for granting access to the dataset and their library for this work. We are also grateful to the field personnel of the Department of Physics (Geophysics Unit), KNUST, Kumasi, Ghana for their support.

References

Affaton, P., Aguirre, L., and Menot, R.-P. (1997). Thermal and geodynamic setting of the Buem volcanic rocks near Tiele,, Northwest Benin, West Africa. *Precambrian Research, 82*, 191-209.

Airo, M. L., & Karell, F. (2001). Interpretation of airborne magnetic and gamma-ray spectrometric data related to Mammaslhti Cu-Zn-Au deposit in eastern Finland. *Special Paper 31* , 97–103.

Airo, M. L., and Loukola-Ruskeeniemi, K. (2004). Characterization of sulfide deposits by airborne magnetic and gamma-ray responses in eastern Finland. *Ore Geology Reviews, 24*(1), 67-84.

Bell, S., & Crook, J. (2003). *The Geology of 1/4 Feild Sheets 182, Hohoe S. E with a contribution on the structural Relationship to Kpandu- Ho Area.* Accra: Ghana Geological Survey Department.

Blay, P. (2003). *The Geology of 1/4 Feild Sheets Nos. 184, 185 and 187, Hohoe N. E., Baglo S.W. and N.W.* Accra: Ghana Geological Survey Department .

Blum , M. (1999.). *Processamento e interpretação de dados de geofísica aérea no Brasil central e sua aplicação à geologia regional e prospecção mineral.* Brasília: Instituto de Geociências. Universidade de Brasília.

Briggs, I. (1974). Machine contouring using minimum curvature. *Geophysics, 39*(1), 39-48.

Dapaah-Siakwan, S., and Gyau-Boakye, P. (2000). Hydrogeologic framework and borehole yields in Ghana. *Hydrogeology Journal, 8*, 405–416.

Delor, C., Fullgraff, T., Urien, P., Le Berre, P., Thomas, E., Roig, J., et al. (2009). *Geological Map Explanation – Map Sheets 0700A/2, 0700B/1, 0800D/1, 0800D/3, 0800C/2 & 0800C/4.* Accra: Geological Survey Department of Ghana (GSD).

Direen, N. G., Lyons, P., Korsch, and Glen, R. (2001). Integrated geophysical appraisal of crustal architecture in the eastern Lachlan Orogen. *Exploration Geophysics, 109*, 136-142.

Dobrin, M., and Savit, C. (1988). *Introduction To Geophysical Prospecting* (Fourth Edition ed.). Singapore: McGraw-Hill.

Elton, L., Adalene , M., Tati , A., and Roberto , A. (2003). Old Geophysical Data Applied To Modern Geological Mapping Problems: A Case-Study in the Seridó Belt, Ne Brazil. *Revista Brasileira de Geociências, 33*(2), 65-72.

Geotech Airborne Limited. (2009). *Integrated Interpretation Report on a Versatile Time Domain Electromagnetic (VTEM) Survey on the Hohoe Project Area*. Geological Survey Department, Accra, Ghana.

Ghana Geological Survey. (2009). *Geological map of Ghana 1:1 000 000.* Geological Survey Dept., Accra.

Gregory, A., and Horwood, J. (1961). *A laboratory study of gamma-ray spectra at the surface of rocks.* Ottowa: Department of Energy, Mines and nnnResources.

Gunn, P. (1997). Regional magnetic and gravity responses of extensional sedimentary Basins. *AGSO Journal of Australian Geology and Geophysics, 17*(2), 115-131.

Gunn, P., Maidment, D., and Milligan, P. (1997). Interpreting aeromagnetic data in areas of limited outcrop. *AGSO Journal of Australian Geology and Geophysics, 17*(2), 175–185.

Jones, W. (1990). The Buem volcanic and associated sedimentary rocks, Ghana: a field and geochemical investigation. *Journal of African Earth Sciences, 11*(3–4), 373-383.

Junner. (1940). The Geology of the Gold Coast and western Togoland. *Gold Coast Geological Survey Bulletin, 11*, 1-40.

Kennedy, W. (1964). *The structural differentiation of Africa in the Pan-African (±500 m.y.) tectonic episode.* UK: Leeds University Institute for African Geology.

Kesse, G. O. (1985). *The Mineral and Rock Resources of Ghana.* A.A. Balkema, Rotterdam.

Ku, C., and Sharp, J. (1983). Werner deconvolution for automated magnetic interpretation and its refinement using Marquart's inverse modeling. *Geophysics, 48*(6), 754-774.

Minty, B. (1997). Fundamentals of airborne gamma-ray spectrometry. *AGSO Journal of Australian Geology and Geophysics., 17*(2), 39-50.

Mushayandebvu, M., van Drielz, P., Reid, A., and Fairhead, J. (2001). Magnetic source parameters of two-dimensional structures using extended Euler deconvolution. *Geophysics, 66*(3), 814–823.

Norman, K. G. (1969). The Late Precambrian to Early Paleozoic Pan-African Orogeny in Ghana, Togo, Dahomey, and Nigeria. *Geological Society of America Bulletin, 80*(1), 45-56.

Oruc, B., and Selim, H. (2011). Interpretation of magnetic data in the Sinop area of Mid Black Sea, Turkey, using tilt derivative, Euler deconvolution, and discrete wavelet transform. *Journal of Applied Geophysics, 74*, 194–204.

Osae, S., Asiedu, D., Banoeng-Yakubo, B., Koeberl, C., and Dampare, S. (2006). Provenance and tectonic setting of Late Proterozoic Buem sandstones of southeastern Ghana: Evidence from geochemistry and detrital modes. *Journal of African Earth Sciences, 44*, 85–96.

Salem, A., Williams, S., Fairhead, J., Ravat, D., and Smith, R. (2007). Tilt-depth method: a simple depth estimation method using first-order magnetic derivatives. *The Leading Edge , 26*, 1502-1505.

Wilford, J. R., Bierwirth, P. N., and Craig, M. A. (1997). Application of airbornegamma-ray spectrometry in soil/regolith mapping and applied geomorphology. *AGSO Journal of Australian Geology and Geophysics, 17*(2), 201–216.

Wright, J., Hastings, D., Jones, W., and Williams, H. (1985). *Geology and Mineral Resources of West Africa.* London: George Allen and Unwin publishers Ltd.